BAA number HR001117S0025

Lead Organization University of Florida

Type of organization Large Organization

Proposers internal reference number

Team members :

PI Jenshan Lin University of Florida
Co-PI Changzhi Li Texas Tech University
Co-PI YK Yoon University of Florida
Co-PI Joaquin Casanova University of Florida

Proposal title Biomimetic microfabricated magnetic gradiometer

Technical PoC :

Joaquin Casanova
1064 Center Dr, 565 NEB, Gainesville, FL 32611
352-246-9649, jcasa@ufl.edu

Administrative PoC :

Steven Blodgett
1064 Center Dr, 216 LAR, Gainesville, FL 32611
352-846-3948, blodgetts@ece.ufl.edu

Total funds requested

Submitted 06/01/2017

Official transmittal letter

The transmittal letter should identify the BAA number, the proposal by name, and the organizations proposal reference number (if any), and should be signed by an individual who is authorized to submit proposals to the Government.

Detailed Proposal Information

1 Statement of Work (SOW)

The project's aim is to develop a minaturized high-sensitivity, low-noise magnetic gradiometer. Our approach is to mimic the mechanism found in magnetosomes, the specialized cells from bacteria to higher vertebrates such as fish and birds (see 2). This is comprised of three main tasks: modeling and simulation, microfabrication process design, and circuit design. Each Phase (1,2,3) will include these three tasks. No task requires the use of government equipment. 'Successful' completion of a design indicates satisfaction of the parameters in Table 1 following the test procedures described in 6. Testing will be completed at UF by Drs. Casanova and Yoon at UF in all phases.

Metric	Phase 1	Phase 2	Phase 3
Power consumption	150 mW	50 mW	100 mW
Sensor Volume	3x3x10 cm	1x1x7 cm	1x1x7 cm
Control Electronics Volume	N/A	N/A	20cm^2
Ambient Magnetic Field	$\pm$ 100 μT	$\pm$ 100 μT	$\pm$ 100 μT
Ambient Operating Temperature	N/A	0° C to 50° C	0° C to 50° C
Gradient Full-scale Range	1 nT/cm	1 nT/cm	1 nT/cm
Gradient Sensitivity	10 fT/cm/$\sqrt{Hz}$	3 fT/cm/$\sqrt{Hz}$	1 fT/cm/$\sqrt{Hz}$
Gradient Accuracy	100 fT/cm	30 fT/cm	10 fT/cm
Total Field Range	100 μT	100 μT	100 μT
Total Field Sensitivity	100 pT/$\sqrt{Hz}$	30 pT/$\sqrt{Hz}$	10 pT/$\sqrt{Hz}$
Total Field Accuracy	1 nT	500 pT	100 pT
Data Rate	100/s	200/s	500/s
3 dB Bandwidth	200 Hz	400 Hz	1000 Hz

Table 1: Design objectives, by phase.

1.1 Phase 1 Tasks

AMBIIENT Phase 1 will demonstrate sensor functionality and performance in a laboratory setting meeting the performance metrics as indicated in Table 1.

1.1.1 Modeling and simulation of biomimetic sensor

The objective in this phase, to be accomplished at UF by Joaquin Casanova, is to simulate the device, taking into account geometry, material properties, and multiphysics interactions, in order to determine the range of acceptable design options for a single element. Multiple options can be fabricated for real-world testing. Our approach here is to initially specify geometry and physical properties by hand calculation, then investigate more deeply in a finite-element multiphysics solver. Completion of this task is specified by successful simulation of the sensor device that meets the physical requirements specified in the BAA, and deliverables include successful simulation results and design parameters. To reduce risk of non-manufacturability, this task will be accomplished

within fabrication constraints specified by the sensor team at UF. This ensures the design is physically realizable. In parallel, other sensing modalities could be explored in the case that the sensor cantilever is not practical.

1.1.2 Microfabrication process design

The objective in this phase, to be accomplished at UF by Dr. YK Yoon, is to develop a microfabrication strategy (materials, deposition, patterning) that can meet the requirements found from simulation. Our approach here is to find a range of dimensional constraints and material types that could be physically realizable, and use those options to guide simulation and design of a sensor. Completion of this task is successful specification and execution of a microfabrication plan for the sensor described by the simulation results and deliverables include successful microfabrication plan and sensor. To reduce risk of later failure due to non-manufacturability, this task will be accomplished with parallel investigating of alternative sensing modalities, and multiple sensor designs can be fabricated for testing.

1.1.3 PCB-based circuit design

The objective in this phase, to be accomplished at TTU by Dr. Changzhi Li, is to develop a PCB-based detection circuit which amplifies and digitizes the the voltage produced by the sensor elements. In addition to a COTS circuit, we will simultaneously begin investigation and design of an SiGe IC that can be used in later phases. Our approach here is to drive the cantilevers at their resonant frequency to enhance sensitivity, amplifying the signal, then demodulate. Banks of sensors will be individually addressable. Completion of this task is specified by successful design and fabrication of a PCB-based circuit capable of amplifying and digitizing sensor output voltage with input-referred voltage noise low enough to meet the overall sensitivity requirement. Deliverables include successful design and prototype of the circuit, usable with the microfabricated sensor head, using COTS components. To reduce risk of later failure due to excessive noise, this task will investigate only specifically low-noise designs. Dynamic element matching will permit cancellation of manufacturing variation cancellation. The Phase 1 circuit will be completed with COTS components.

1.2 Phase 2 Tasks

AMBIIENT Phase 2 will develop and demonstrate an integrated sensor head meeting the performance and SWaP metrics of Table 1, and including all vacuum, photonic, and thermal control components.

1.2.1 Modeling and simulation of sensor banks with improved performance

The objective in this phase, to be accomplished at UF by Joaquin Casanova, is to optimize the sensor design by decreasing size, and increasing sensitivity, and constructing in arrays, based on results from the Phase 1. Phase 1 measured results will be compared to simulation to refine accuracy of simulations and account for effects that may not have been considered. Our approach here is to first compare measured vs. simulated results, update our simulations, and then use the refined model to optimize a new design. Completion of this task is specified by successful simulation of

the device that meets the physical requirements specified in the BAA for Phase 2. Deliverables include successful simulation results and design parameters. To reduce risk of later failure due to non-manufacturability, this task will be accomplished within fabrication constraints specified by the microfabrication team at UF, and considering the results of the Phase 1 testing. This ensures the design is physically realizable and modeling is accurate.

1.2.2 Microfabrication of revised sensor head

The objective in this phase is to optimize the microfabrication process, through material selection and process design, considering problems encountered in Phase 1. Our approach here is to improve the material selection and process design over Phase 1, in conjunction with Phase 2 simulations. For instance, incorporating higher-energy magnetic materials, or denser interconnects. This task will be accomplished at UF by YK Yoon. Completion of this task is specified by successful fabrication of the Phase 2 sensor design and delivery of a microfabricated sensor, with pads for connection to the Phase 2 circuit. To reduce risk of later failure due to non-manufacturability (as a result of interconnect density, or damping effects, for instance), this task will also investigate an architecture with fewer, larger sensors.

1.2.3 Circuit design and integration

The objective in this phase, to be accomplished at TTU by Changzhi Li, is to optimize the PCB-based circuit based on the Phase 1 results and test this with a sensor array, and incorporate the amplifier design into an integrated circuit, for testing with the Phase 2 sensor array. Our approach here is to take the Phase 1 circuit design, altering it based on the modified sensor design, and design from this an integrated circuit, to reduce size. SiGe is a likely process choice due to low noise. Completion of this task is specified by successful design and fabrication of a sensor amplification IC. To reduce risk of later failure due to missing deadlines, or circuit/sensor mismatch, preliminary IC design will begin in Phase 1. Additionally, multiple designs can be incorporated into one IC.

1.3 Phase 3 Tasks

AMBIIENT Phase 3 will demonstrate a fully integrated gradiometer comprising all control electronics, power conditioning, and packaging, meeting all performance metrics of Table 1

1.3.1 Modeling and simulation of revised and optimized micro sensor

The objective in this phase is to optimize the sensor, to decrease size and increase sensitivity, based on results from the Phase 2. Phase 2 measured results will be compared to simulation to refine accuracy of simulations and account for effects that may not have been considered. The Phase 3 design will be completed with circuit integration specifically in mind. Dr. Casanova will first compare measured vs. simulated results, update our simulations, and then use the refined model to optimize a new design. Completion of this task is specified by successful simulation of the sensor that meets the physical requirements specified in the BAA for Phase 3. To reduce risk of later failure due to non-manufacturability, this task will be accomplished within fabrication constraints specified by the team at UF, and considering the results of the Phase 2 testing. This ensures the design is physically realizable and modeling is accurate.

1.3.2 Microfabrication of final sensor design

The objective in this phase is to optimize the microfabrication process, through material selection and process design, considering problems encountered in Phase 2. To acomplish this, Dr. Yoon will improve the material selection and process design over Phase 2, in conjunction with Phase 2 simulations. For instance, incorporating higher-energy magnetic materials, or denser interconnects. Additionally, the Phase 3 sensor and Phase 3 circuit will be integrated into the same substrate, and packaged. The Phase 3 IC will be sliced and bonded onto a common substrate with the sensor. This task will be accomplished at UF by YK Yoon and at TTU by Changzhi Li. Completion of this task is specified by successful fabrication of the Phase 3 sensor design and will result in a successful IC, with integrated Phase 3 sensor. To reduce risk of later failure because the IC and sensor can't be integrated as part of the same substrate, we will also pursue the option of completing each separately and connecting.

1.3.3 Complete integrated circuit design

The objective in this phase is to optimize the SiGe IC based on the Phase 2 results and refined Phase 3 design, and full-scale integration of the IC and sensor array. Our approach here is to take the Phase 2 circuit design, modifying based on the modified sensor design, adding an ADC, and design from this a single integrated circuit, to reduce size. This task will be accomplished at TTU by Changzhi Li. On completion of this task, Dr. Li will deliver a successful design in simulation and fabricate a sensor amplification IC. To reduce risk of later failure due to missing deadlines, or circuit/sensor mismatch, preliminary Phase 3 IC design will begin in Phase 2. Additionally, multiple designs can be incorporated into one IC.

2 Innovative Claims

Our approach is to design a sensor based on a magnetoreceptive mechanism used in nature - magnetite crystals torqued by external magnetic fields open ion channels in the cell wall. To mimic this, we propose a microfabricated sensor, with a layer of magnetic material on top of piezo electric cantilevers. When forced with an exernal field, torque induced on the magnet creates stress in the piezo, and thus a voltage is produced. **There are three advantages to this approach. First, microfabrication allows for a small size. Second, by orienting individual sensing elements in anti-series order, the output is natively a gradiometer. Third, by selecting the resonant frequency of the cantilever carefully, we can create a gradiometer which outputs a spectrogram directly.** Though fluxgates can be microfabricated and function as gradiometers, they suffer a size/sensitivity tradeoff. Microfabricated atmonic magnetometers are sensitive but don't function natively as gradiometers. Other micro-scale magnetometers, namely Lorentz-type, which operate on a similar mechanism, are not yet sensitive enough and haven't been used as frequency-domain gradiometers, as in the proposed design.

3 Detailed Technical Approach

3.1 Motivation and previous work

Magnetometers serve an important role in investigating biologically generated electromagnetic fields, such as those created by neuronal currents, or geological magnetic fields. Typically, magnetometers are unable to achieve high sensitivity in an ambient, unshielded environment - getting to femtotesla level sensitivity requires magnetic shield and cryogenic sensors, such as SQUID [20]. The novel spin relaxation free magnetometer has been minaturized and achieves less than 10 fT/$\sqrt{Hz}$, but still requires shielding and lacks directional sensitivity [26]. Fluxgates have achieved pT level resolution at small size, but this is insufficient for biomagnetic field measurement [24, 25, 31]

Lorenz-type magnetometers (which translate magnetic fields into mechanical actuation of a magnet or current carrying wire) have been built in MEMS substrates, but are as yet insufficiently sensitive and require shielding [18, 19, 28, 30]

Three of the proposers (Drs. Lin, Li, and Casanova) have been involved in previous DARPA work on the Mind Electromagnetic Localization Device (MELD) project, which involved designing, fabricating, and testing low-field magnetometers and the concomitant circuitry and software. Our experience in this field has given us useful experience and equipment, so we are familiar already with this pitfalls and challenges associated with the previously mentioned approaches. Dr. Yoon has direct experience in developing advance microfabrciation processes and applications ([35, 38]), leading us to consider a different approach: mimicking the magnetometry found in nature on the cellular level.

In nature, many organisms have a sense of magnetoreception used for navigation, from magnetotactic bacteria to birds. Two mechanisms have been proposed: a spin-selective (and thus field-sensitive) chemical reaction rate, or magnetite crystals which are actuated by external fields and activate ion channels in the cell membrane (Figure 1) [9, 14, 17]. Measurements of these magnetosomes show a magnetic dipole moment of up to 100fA/m^2 [11, 12].

3.2 Biomimetic sensor design

Our approach is to mimic the approach found in magnetosomes, with some key modifications so that is frequency-selective and functions inherently as a gradiometer and thus does not require shielding. The closest biomimetic sensor is a flow sensor which uses ferromagnetic cilia to detect microfluidic flow rates [1].

To acomplish this, we propose layering a permanent magnetic layer on top of piezoelectric cantilevers. The torque induced on the magnetic layer generates stress in the piezo layer, and thus a voltage and charge. For an estimate of the sensitivity of this type of sensor, we perform a basic analysis. The moment N induced on the magnetic layer with moment $\vec{m}$ and field $\vec{B}$ is:

$$N = \vec{m} \times \vec{B}$$

Interpreted as a point load (N/L) at the cantilever tip, this moment causes a stress distribution on a cantilever of length L, thickness t, second moment I, piezoelectric voltage constant g_{31}, and modulus E, at point (x,y), of

$$\sigma = \frac{Ny(L-x)}{LI}$$

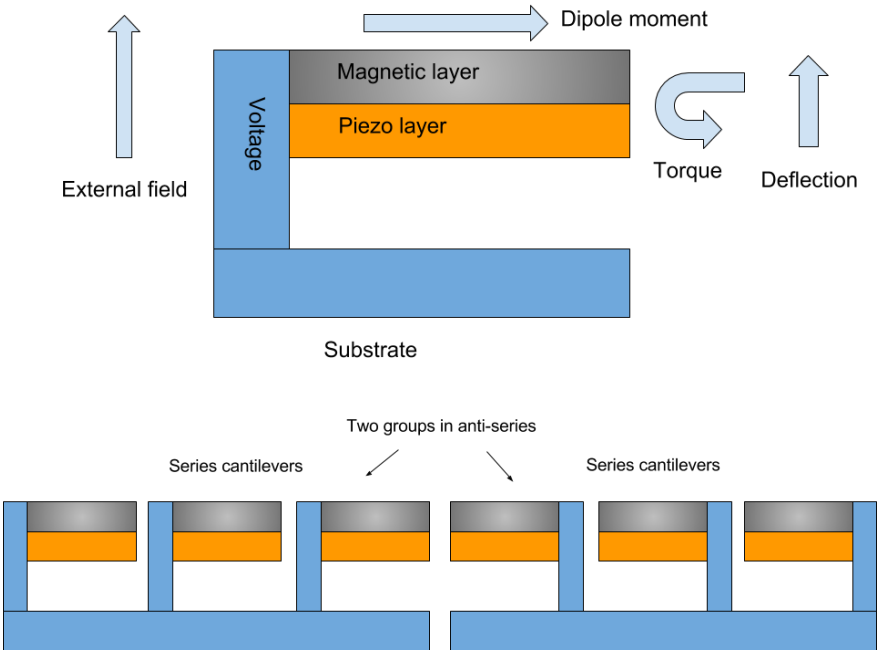

Figure 2: Diagram of proposed design.

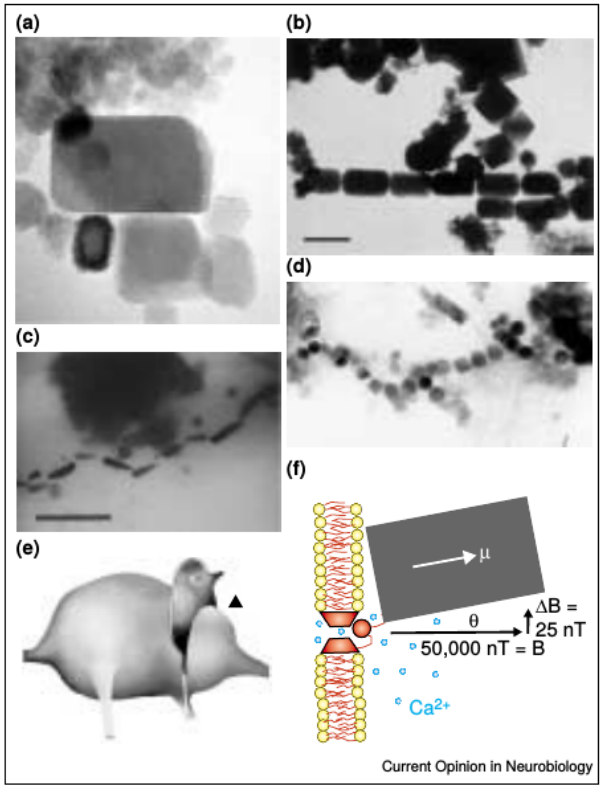

Figure 1: Magnetosomal mechanism [17].

and n in series generates a voltage

$$V = \frac{\int_0^L \int_{-t/2}^{t/2} \left| \frac{Ny(L-x)}{LI} g_{31} n \right| dydx}{L}$$

Two features are possible from the cantilever design: frequency selection and gradiometery. As in [27], a cantilever has a resonant frequency, which can be modified through geometrical parameters. Peak response will be achieved at this frequency. By selecting many cantilevers of different dimensions, each corresponding to a separate output, the magnetometer output is a spectrometer. Many cantilevers at the same resonance in series generate a larger voltage; in anti-series, the difference is taken, thus functioning as a gradiome-

ter with very high spatial resolution (Figure 2).

The noise floor of magnetic materials is governed by Barkhausen noise - the random flipping of magnetic domains [3]; this noise is characterized as a flux noise level. The flux noise can be converted into a magnetic moment noise, and thus moment noise. Piezo noise floor is largely a function of piezo losses [21]. Additionally, there is the input-referred noise of any amplifier. With conservative estimates for all of these, and two anti-series banks of 30 cantilevers each with dimensions 400x40x3 μm, the sensitivity level is less than 10 fT/cm/$\sqrt{Hz}$.

Even though biological magnetoreception is limited to nT sensitivity, our design will allow us to surpass this. First, by careful selection of materials (such as Co-Pt or rare-earth magnets) [2,8] we can have much higher magnetic dipole moment, and thus higher moment. Second, by careful selection of geometry, we can employ parametric resonance [32]. Third, by using many elemens in series and summing, we can increase signal-to-noise ratio (SNR). Finally, using two banks of series cantilevers in anti-series, we both boost the voltage and create a high resolution gradiometer.

Some potential pitfalls include effects of viscous damping (limiting mechanical vibration at resonance), demagnetization factor (due to the particular geometry of the magnetic layer), and layer separation from stress differentials (if strain at the interface betwwen layers is not equal, they can peel apart). To assess these more closely, multiple physical effects, with non-linear, anisotropic materials must be considered simultaneously, for a complex geometry. A large part of the MEMS sensor design process must therefore be completed in simulation, allowing us to determine the impact of the above effects. Additionally, we can optimize the geometry and material selection for maximum reponse. Key design variables include the coercivity and remanance of the magnetic layer, the piezoelectric coefficients of the piezoelectric layer, the Young's modulus of each, and the length, width, and thickness of the cantilever. The physics of the system can be described by the PDEs for magnetostatics, mechanical deformation, and the piezoelectric constitutive relations:

$$\nabla \vec{B} = 0$$

$$\vec{B} = \mu_o(\vec{H} + \vec{M}(\vec{H}))$$

where $\vec{B}$ is the magnetic flux,$\vec{H}$ the sum of external and internal fields, and $\vec{M}$ the magnetization.

$$-\nabla \cdot \vec{\sigma} = \vec{f}$$

$$\vec{\sigma} = \lambda(\nabla \cdot u)I + \mu(\nabla u + (\nabla u)^T)$$

$$\vec{f} = -\nabla \times \vec{N}$$

$$\vec{N} = \vec{m} \times \vec{B_{ext}}, \vec{m} = \vec{M}$$

where $\vec{N}$ is the moment per volume, $\vec{f}$ is force per volume, $\vec{u}$ is displacement of the beam, λ and μ are Lame elasticity parameters, $\vec{m}$ is magnetic moment per volume, and $\vec{\sigma}$ is the stress tensor.

Finally, to relate field $\vec{E}$, strain $\vec{S}$, displacement field $\vec{D}$, and stress $\vec{\sigma}$, in the piezo layer:

$$S_{ij} = s_{ijkl}\sigma_{kl} + d_{kij}Ek$$

$$D_i = d_{ikl}\sigma_{kl} + \epsilon_{ik}E_k$$

Together, these relations allow us to estimate resonance, stress, and sensitivity of our sensor. FeniCS provides an open-source finite-element multiphsics solver [10]; though less user-friendly, it is flexible, and free, and sufficient for our needs.

3.3 Microfabrication process

Microfabrication processes are capable of constructing the above-described sensor. The process consists of two main fabrication tasks: piezoelectric cantilever construction and magnetic material integration. Zinc oxide (ZnO) has a high strain-to-voltage coefficient in both the 31 and 33 directions and is highly suitable for piezoelectric sensors [29]. It is also bio compatible, and environmentally friendly. ZnO is typically deposited with sputtering or solution-based deposition techniques [39] and patterned with chemical or ion etching.

Rare-earth magnetic materials, such as alloys of Sm-Co, offer high magnetic energy products at room temperature and can be integrated into MEMS using sputtering or pulsed lased deposition (PLD) [2]. However, patterning of these materials is slow, using wet etching or ion-beam milling. Additionally, thick films or high aspect ratio structures composed of these materials become difficult, mainly due to the lack of a suitable electroplating process. To solve this problem, it is possible to embed a rare earth transition metal magnetic material, such as NdFeB, in a resin, then use a mold to pattern the magnetic resin composite [33]. Additionally, transition metal magnetic materials, such as FePt or CoPt, can be electroplated and also show relatively high magnetic energy products at room temperature [2, 4].

Our proposed fabrication procedure is similar to others in MEMS [27]. The process involves six masks with one being a backside mask. The process will require double sided polished wafers, but the p+ etch stop removes the need for SOI wafers. However, if the doping process does not give the needed uniformity, SOI wafers may be used as well. Alternatively, if the KOH etching is too rough or if smaller spacing between columns is needed, reactive ion etching (RIE) may be used for the backside etch. The electrode area is patterned separately from the cantilevers since the accuracy of both the alignment and etching is not nearly as high. The detail fabrication steps are as follows:

1. Deposit silicon oxide using plasma enhanced chemical vapor deposition (PECVD) and pattern bottom electrode materials (titanium and platinum: Ti/Pt) with RIE etching according to the first mask in the electrode area (Fig. 4(a))

2. Deposit the piezoelectric material (ZnO) and pattern with wet etching according to the second mask in the electrode area (Fig. 4(a))

3. Deposit the top electrode material (Ti/Pt) and pattern with liftoff according to the third mask in the electrode area (Fig. 4(a))

4. Use RIE to etch the layers deposited in the preceding steps to define the cantilever with the forth mask (Fig. 4(b))

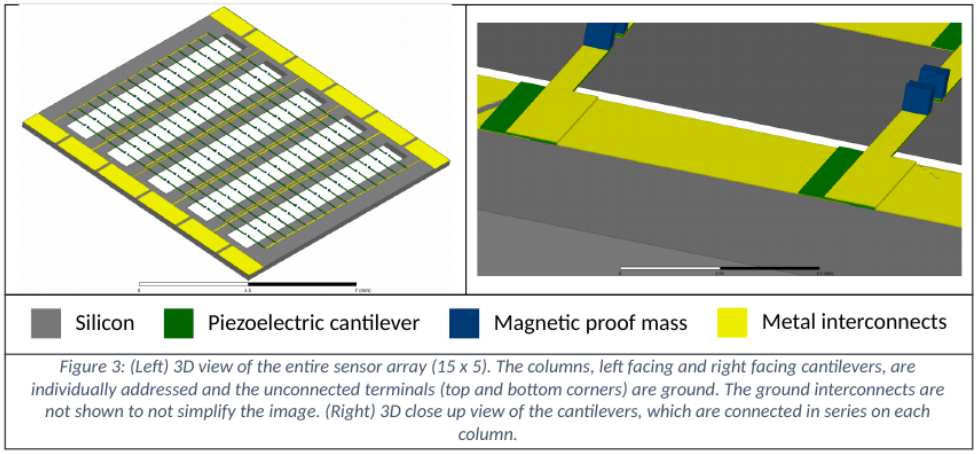

Figure 3: (Left) 3D view of the entire sensor array (15 x 5). The columns, left facing and right facing cantilevers, are individually addressed and the unconnected terminals (top and bottom corners) are ground. The ground interconnects are not shown to not simplify the image. (Right) 3D close up view of the cantilevers, which are connected in series on each column.

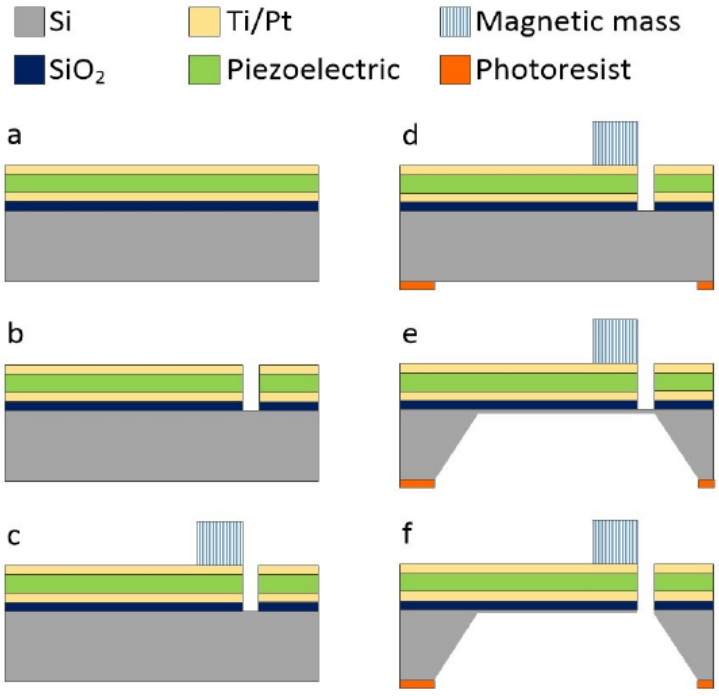

Figure 4: Magnetic cantilever fabrication. The patterning associated with steps 1-3 of the process described in the text are not shown due to image complexity and are represented by (a)

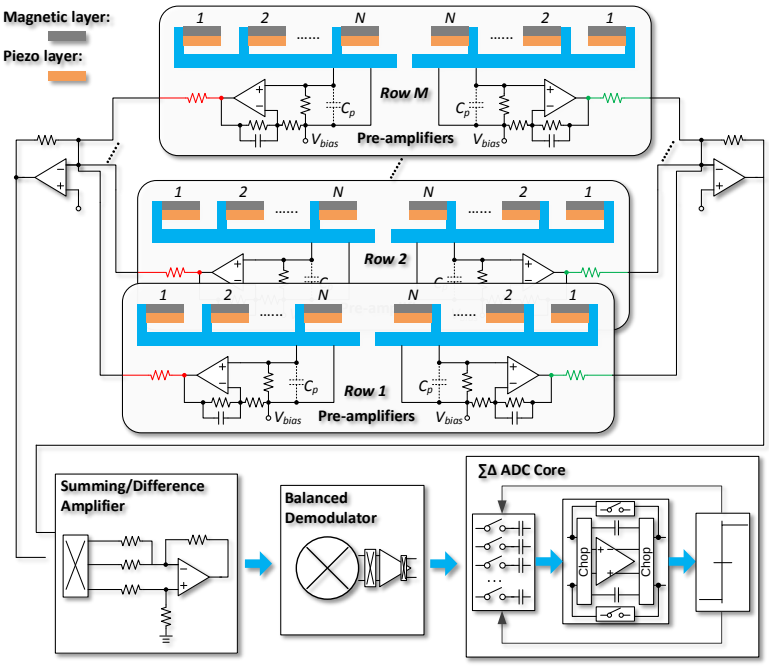

Figure 5: System design.

5. Deposit the magnetic proof mass using the mold approach (NdFeB) or electroplating (FePt or CoPt) with the fifth mask (Fig. 4(c))

6. Use backside exposure to pattern the backside of the silicon according to the sixth mask (Fig. 4(d))

7. Etch the backside of the silicon using KOH with a p+ epilayer as an etch stop (Fig. 4(e))

8. Release the cantilevers with a selective frontside RIE (Fig. 4(f))

3.4 Circuit design

From circuits and systems point of view, this could be modeled using a very-large-scale oversampling sensing architecture. A simple example is laid out as follows:

Assuming a sensor of area A generates a signal of S, and it has intrinsic noise of N_i. In comparison, two sensors each with an area of $A/2$ would each generate a signal of $S/2$ and noise of $N_i/2$. When the two $A/2$ sensors are combined, their total signal will be S. But since the noises from the two $A/2$ sensors are uncorrelated, the combined total noise will be:

$$\sqrt{(N_i/2)^2 + (N_i/2)^2} = N_i/\sqrt{(2)}$$

Therefore, splitting a sensor into two with equal sizes will result in a factor of $\sqrt{2}$ increase in the signal-to-noise ratio (SNR). Likewise, splitting a sensor into an array of M small units that sum up to the same total size would lead to a factor of $\sqrt{2}$ increase to the SNR. Because of this

oversampling gain to the SNR, magnetosomes with thousands of magnetite crystals are able to have a superb sensitivity to small fluctuations of magnetic field, which can hardly be achieved by conventional man-made tools.

Ideally, if a sensor can be split into an infinite number of miniaturized elements, it would approach the capability of magnetosomes to achieve ultra-high field sensitivity. On the other hand, it is the most desirable to implement this bio-inspired oversampling mechanism in the analog front-end because any added back-end circuitry would introduce parasitics and noise that would otherwise hinder the effectiveness of the ideal oversampling theory. Inspired by this bio-mechanism of oversampling, we propose to combine the magnetic/piezo cantilevers in groups, and use low-noise amplifiers to pick up signals directly from the elements. The low-noise amplifiers will be reconfigurable in summing and difference modes to detect total field and field gradient. An overview of the system is shown in 5.

Voltage-mode and charge-mode amplifications are two main approaches to signal conditioning of piezoelectric sensors. Voltage-mode amplification is useful when the amplifier is very close to the sensor and thus minimal parasitic capacitance is presented by the interconnection between the sensing device and the amplifier input. Charge-mode amplification is useful when the amplifier is remote to the sensor because it is robust against parasitic capacitance of interconnections. Depending on the characterization and optimization of the MEMS device front-end, the team is ready to investigate both approaches and fully integrate the final solution with special circuit techniques for the optimal performance.

3.4.1 Voltage-mode approach

The simplified structure for voltage-mode amplifiers is depicted in Fig. 5, represented by the circuits that directly interface with each row of the MEMS device. Depending on the fabricated and optimized MEMS size, either one or multiple amplifiers in parallel will be implemented for each row to collect the piezoelectric voltage signal. The goal of using multiple amplifiers in parallel is to enhance the SNR because of the benefit of oversampling. However, constraint exists due to the area available under the MEMS device. The circuit team will work closely with the device team in this project to determine the ideal placement of local voltage-mode amplifiers in Phase I of this project, and compare the performance with the charge-mode approach discussed next.

3.4.2 Charge-mode approach

Charge-mode amplifier approach will also be investigated because it has advantages in handling interconnect parasitics and the convenience of adding signals from different rows of the MEMS device together. Inspired by existing works in neural recording [13], the team will use MOS-bipolar pseudo-resistors as the feedback resistors in the charge-mode amplifier. As shown in Fig. 6, two back-to-back connected PMOS transistors (T1 and T2) that can easily achieve resistance of GOhm will be implemented as the feedback resistor of the charge-mode amplifier, enabling processing brain signals with a frequency as low as 0.025 Hz. With negative VGS, T1 and T2 function as diode-connected PMOS transistors. With positive VGS, the parasitic sourcewelldrain p-n-p bipolar junction transistor (BJT) is activated, such that T1 and T2 act as diode-connected BJTs. For small voltages across the pseudo-resistors, the small-signal resistance is extremely high and thus moves the corner frequency to low enough for bio-signal processing. On the other hand, a large voltage across the pseudo-resistors will reduce the small-signal resistance and result in a fast settling time

for the amplifier. As a result, this pseudo-resistor-based design can amplify low-frequency signals down to the millihertz range while properly rejecting large DC offsets. The theoretical noisepower tradeoff limit, i.e., the noise efficiency factor, have already been derived and demonstrated by selectively operating MOS transistors in either weak or strong inversion [13]. The only potential drawback of this configuration is that the amplifier cannot have a large output swing, because otherwise the pseudo-resistors may become two diodes. However, this is not a concern for this work as the amplifier is implemented as pre-amplifier in the front-end, where signal to be handled is very weak.

3.4.3 Re-configurable summing and difference amplifiers

After the piezoelectric signal is captured by arrays of preamplifiers located near the MEMS devices, the obtained voltage signals will be further processed by a re-configurable summing and difference amplifier. This amplifier will be digitally controlled in real-time to either add or subtract signals coming from different regions of the fabricated device. This will enable both common-mode detection, which senses the total field, and differential-mode detection, which senses the field gradient.

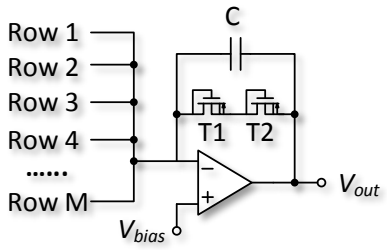

Figure 6: Charge-mode amplifier with pseudo-resistor feedback and summing capability.

One potential challenge for the summing and difference amplifier is the tradeoff between high sensitivity and large dynamic range. Being able to perform both summing and difference detection, as well as the existence of strong earth field, requires the amplifier to have a very large dynamic range. However, the DARPA specification also mandate high sensitivity for brain signal recovery. To this end, a 3-op-amp topology will be customized and implemented in GlobalFoundries 180-nm SiGe BiCMOS 7WL process for both low-noise and high-linearity operation. Bipolar PNP transistors will be utilized as the input buffer to minimize the input-referred noise. A programmable resistor array will be implemented between the outputs of the two first-stage amplifiers to provide a large tunable gain range. In a previous DARPA project (MELD Mind Electromagnetic Localization Device), the team has evaluated various topologies and different semiconductor processes (e.g., SOI versus BiCMOS) for the amplifier of brain magnetic field detector, and verified through both Cadence simulation and fabricated chip measurement that the 3-op-amp topology with bipolar transistor input buffer offers the best combined sensitivity and linearity performance.

3.4.4 Solution to low-frequency noise and device mismatch in electronics

Because the magnetic field induced by brain activities not only is extremely weak, but also has very low frequencies (below 100 Hz), 1/f noise and device mismatch have significant impact to the success of the proposed work. To resolve the challenge, the bio-inspired MEMS device will operate at a resonant frequency which carries the signal of interest. A double-balanced demodulator featuring low noise at the baseband output, high rejection to harmonic distortion, and low LO/RF leakage

will be implemented after the summing/difference amplifier to recover the field information of interest.

After the signal is demodulated to the baseband, circuit techniques including dynamic offset cancellation, dynamic element matching (DEM), and chopping will be applied extensively to the remaining signal processing circuits to cancel the mismatch errors and low-frequency noises. On the data acquisition side, the analog-to-digital converter (ADC) is an important component for correctly interpreting the field information. Nyquist ADC accuracy is limited by the matching of components in ADCs, while oversampling ADCs, such as sigma-delta ADC, trade speed for resolution. Because brain signals have low frequencies, sigma-delta ADC is a very good candidate for precision sensing. Another advantage of sigma-delta ADC is that chopping technology and dynamic element matching are suitable for its architecture to minimize the impact of low-frequency noise and offset errors.

4 Risk Analysis and Mitigation Plan

Risk	Probability	Impact	Plan
Insufficient sensitivity in simulation	3	10	Optimize design architecture.
Best available MEMS processes infeasible	4	10	Begin design process within constraints of available processes.
Interconnects infeasible	3	5	Operate fewer, larger cantilevers
Viscous damping hurts sensitivity	3	5	Operate in vacuum packaging
Resonance frequency infeasibly high	3	5	Operate fewer, larger cantilevers
Fabrication unreliable/mismatch	3	5	Begin fabrication early, so process can be adjusted; dynamic element matching.
Sensitive to mechanical vibration	3	5	Use additional, non-magnetic cantilevers to cancel mechanical vibrations.

Table 2: Risk matrix

There are several risks and challenges associated with this design. Most can be addressed simply by doing careful analysis of the problem within the range of constraints on materials and processes. Others (the density of interconnects, or resonant frequency being too high) can be addressed by reducing the number of elements and increasing their size. Damping due to the viscosity of air that may hurt sensitivity could be addressed by vacuum packaging the sensor head. Manufacturing mismatch of the sensing elements can be effectively removed by dynamic element matching, where the transducers are switched electronically to average out fabrication differences.

5 Schedule and Milestones

Phase	Milestone
1	Cantilever simulation and design
1	Microfabrication
1	Circuit design
1	Testing
2	Cantilever simulation and design
2	Microfabrication
2	Circuit design
2	Testing
3	Cantilever simulation and design
3	Microfabrication
3	Circuit design
3	Testing

Table 3: Milestones schedule

Include a high-level Gantt chart outlining major technical tasks and measureable milestones by phase. At a minimum, the schedule should include each SOW task of Volume 1, Section II.A. Where risk reduction tasks are proposed, the schedule should include a milestone for assessment and removal of redundant tasks.

6 Test Plan

To test, in Phase 1, the sensor will first be connected to the circuitry and powered to established basic functionality. Prior to testing, noise from the Helmholtz coils, power supplies, and any other necessary signal generation sources will be characterized. Further, the sensor will be placed in a pair of Helmholtz coils driven with precision current sources, inside magnetic shield, so we can gauge accuracy and sensitivity in a controlled environment. Field gradient, intensity, and frequency will be swept over the range specified in 1. Finally, the same test will be repeated in an unshielded environment. In each case, we will monitor power consumption, signal output, and mesure sensor and sensor control electronics volume. Subsequent phases will follow a similar testing protocol, except using specifications for those phases. Additionally, in Phases 2 and 3, where an IC will be developed and integrated with the sensor head, the IC will be tested independently to verify basic input/output functionality before slicing and bonding to the MEMS substrate.

7 Results and Technology Transfer

Our research team has demonstrated successful technology transfer to the government and private sectors in our work on wireless power, vital signs radar, and low-field magnetometry. UF's Office of Technology Licensing is very helpful in patenting and licensing new engineering developments from research.

The proposed work is highly amenable to technology transfer. The sensor and circuit design is novel and likely patentable, even if it fails to meet all requirements in the BAA. This can be considered fundamental research and thus not ITAR-controlled. Further, there is no private industry involvement, so any technology transfer is just between UF and DARPA.

8 Ongoing Research

Presently, Drs. Lin, Li, and Casanova are involved (until 6/2017) in a DARPA project for detection and inversion of MEG/EEG signals. They have worked on all phases, from sensor design to circuit design to inversion algorithm. Additionally, Drs. Lin and Li have worked exensively on vital signs radar, and Dr. Casanova has worked on electromagnetic sensors for agriculture and analytical chemistry. Dr. Yoon has conducted research in MEMS systems of all types, including piezoelectronics and magnetics.

9 Facilities

Facilities at UF for sensor development and testing include magnetic shielding, circuit testing instrumentation (power supplies, oscillopes, function generators, VNA). For fabrication, the Nanoscale Research Facility at UF includes equipment for a variety of processes: plasma, vapor, and sputtering deposition, annealing, wafer bonding, wire bonding, UV and e-beam lithography, reverse ion etching, and wet etching.

Dr. Lis research group at the Texas Tech University is located in a fully ESD-protected Microwave and Analog Circuits Laboratory. The PI has obtained full support from the Texas Tech University Provost Office and Electrical and Computer Engineering Department to establish this well-equipped lab and enhance the departments research strength on the microwave, and analog circuits. Equipment includes high-frequency network analyzers, signal generators, spectrum analyzer, and oscilloscopes; software useful to this project includes Cadence, Altium, MATLAB, and Labview.

10 Teaming/Proposer Accomplishments

UF The UF team incluldes the following personnel:

Jenshan Lin will be project lead, and supervise work on the AMBIIENT project. His time commitment is 15%. He received the B.S. degree in Electrophysics from National Chiao Tung University (NCTU), Hsinchu, Taiwan, R.O.C., in 1987, and the M.S. and Ph.D. degrees in Electrical Engineering from the University of California at Los Angeles (UCLA), in 1991 and 1994, respectively. His current research interests include sensors and biomedical applications of microwave and millimeter-wave technologies, wireless energy transfer and conversion, RF system-on-chip integration, and integrated antennas. Dr. Lin has authored or co-authored over 250 technical publications in refereed journals and conference proceedings. He holds 15 patents and has several other patent applications. Since joining University of Florida, he has graduated 22 PhD students.

Joaquin Casanova will conduct electromagnetic simulation and design of the MEMS sensor, and work with Dr. Yoon on process/material selection, and Dr. Li on requirements for the interface and control circuits. His commitment is 15%. He received a B.S. and M.E. in Agricultural and Biological engineering in 2006 and 2007 from UF, and PhD in Electrical Engineering in 2010 from UF. His work has primarily focused on sensors and electromagnetic design, including wireless power, microwave remote sensing, agricultural sensors, analytical chemistry equipment design, and low-field magnetic sensing. He is currently a Research Assistant Professor in UF's Department of Electrical and Computer Engineering.

YK Yoon will guide selection of a microfabrication process and fabrication of the sensor. His commitment is 15%. He received his BS and MS degrees in electrical engineering from Seoul National University in Korea. He also earned an MSEE degree from the New Jersey Institute of Technology, Newark, NJ in 1999 and the Ph.D. degree in electrical and computer engineering from the Georgia Institute of Technology, Atlanta, GA in 2004. He is currently an Associate Professor in the Department of Electrical and Computer Engineering at the University of Florida, Gainesville, FL. Dr. Yoon has direct experience in the development of MEMS resonator based magnetic sensors [5–7], and strong expertise in microfabrication [35], piezoelectric [34], ferroelectric [16, 37, 38], ferromagnetic [22, 23, 36], and multiferroic devices [15, 36]. His current research interests include three dimensional (3-D) micromachining and nano fabrication; design and implementation of metamaterial for radio frequency (RF) and microwave applications; micromachined millimeter wave and terahertz antennas and waveguides; bio/microfluidic systems for the lab-on-a-chip applications; wireless telemetry systems for biomedical applications; and ferroelectric material development for high density memory devices and/or tunable RF devices.

TTU The TTU team includes:

Changzhi Li will design the electronics for amplifying and digitizing the signals from the sensor head, working with Dr. Casanova to determine ciruit requirements. His time commitment is 15%. He received the B.S. degree in electrical engineering from Zhejiang University, China, in 2004 and the Ph.D. degree in electrical engineering from the University of Florida, Gainesville, FL, in 2009. In the summers of 2007 and 2008, he worked at Alereon Inc., Austin, TX, on ultrawideband (UWB) transceiver. In the summer of 2009, he worked at Coherent Logix Inc., Austin, TX, on software-defined radio. His research interests include analog circuits, microwave circuits, and biomedical applications of microwave/RF.

Additional Information

References Cited

[1] Ahmed Alfadhel, Bodong Li, Amir Zaher, Omar Yassine, and Jürgen Kosel. A magnetic nanocomposite for biomimetic flow sensing. *Lab on a Chip*, 14(22):4362–4369, 2014.

[2] David P Arnold and Naigang Wang. Permanent magnets for mems. *Journal of microelectromechanical systems*, 18(6):1255–1266, 2009.

[3] Mattia Butta and Ichiro Sasada. Sources of noise in a magnetometer based on orthogonal fluxgate operated in fundamental mode. *IEEE Transactions on Magnetics*, 48(4):1508–1511, 2012.

[4] Tsung-Shune Chin. Permanent magnet films for applications in microelectromechanical systems. *Journal of Magnetism and Magnetic Materials*, 209(1):75–79, 2000.

[5] Seungkeun Choi, S-H Kim, Y-K Yoon, and Mark G Allen. A magnetically excited and sensed mems-based resonant compass. *IEEE transactions on magnetics*, 42(10):3506–3508, 2006.

[6] Seungkeun Choi, S-H Kim, Y-K Yoon, and Mark G Allen. A magnetically excited and sensed mems-based resonant compass. *IEEE International Magnetics Conference (Intermag), San Diego, CA*, 2006.

[7] Seungkeun Choi, Yong-Kyu Yoon, Seong-Hyok Kim, and Mark G Allen. Nonlinear sensitivity enhancement of resonant microsensors and its application to low power magnetic sensing. *Journal of Micromechanics and Microengineering*, 21(4):045004, 2011.

[8] John MD Coey. *Magnetism and magnetic materials*. Cambridge University Press, 2010.

[9] Charlotte A Dodson, PJ Hore, and Mark I Wallace. A radical sense of direction: signalling and mechanism in cryptochrome magnetoreception. *Trends in biochemical sciences*, 38(9):435–446, 2013.

[10] Todd Dupont, Johan Hoffman, Claus Johnson, Robert C Kirby, Mats G Larson, Anders Logg, and L Ridgway Scott. The fenics project. Technical report, Tech. Rep. 2003–21, Chalmers Finite Element Center Preprint Series, 2003.

[11] Stephan HK Eder, Hervé Cadiou, Airina Muhamad, Peter A McNaughton, Joseph L Kirschvink, and Michael Winklhofer. Magnetic characterization of isolated candidate vertebrate magnetoreceptor cells. *Proceedings of the National Academy of Sciences of the United States of America*, pages 12022–12027, 2012.

[12] Marianne Hanzlik, Michael Winklhofer, and Nikolai Petersen. Pulsed-field-remanence measurements on individual magnetotactic bacteria. *Journal of Magnetism and Magnetic Materials*, 248(2):258–267, 2002.

[13] Reid R Harrison and Cameron Charles. A low-power low-noise cmos amplifier for neural recording applications. *IEEE Journal of solid-state circuits*, 38(6):958–965, 2003.

[14] Sönke Johnsen and Kenneth J Lohmann. The physics and neurobiology of magnetoreception. *Nature Reviews Neuroscience*, 6(9):703–712, 2005.

[15] Kyoung-Tae Kim, Cheolbok Kim, Sheng-Po Fang, and Yong-Kyu Yoon. Room temperature multiferroic properties of (fex, sr1- x) tio3 thin films. *Applied Physics Letters*, 105(10):102903, 2014.

[16] Kyoung-Tae Kim, Cheolbok Kim, David E Senior, Dongsu Kim, and Yong-Kyu Yoon. Microwave characteristics of sol-gel based ag-doped (ba 0.6 sr 0.4) tio 3 thin films. *Thin Solid Films*, 565:172–178, 2014.

[17] Joseph L Kirschvink, Michael M Walker, and Carol E Diebel. Magnetite-based magnetoreception. *Current opinion in neurobiology*, 11(4):462–467, 2001.

[18] Varun Kumar, Mohammad Mahdavi, Xiaobo Guo, Emad Mehdizadeh, and Siavash Pourkamali. Ultra sensitive lorentz force mems magnetometer with pico-tesla limit of detection. In *Micro Electro Mechanical Systems (MEMS), 2015 28th IEEE International Conference on*, pages 204–207. IEEE, 2015.

[19] Jukka Kyynäräinen, Jaakko Saarilahti, Hannu Kattelus, Anu Kärkkäinen, Tor Meinander, Aarne Oja, Panu Pekko, Heikki Seppä, Mika Suhonen, Heikki Kuisma, et al. A 3d micromechanical compass. *Sensors and Actuators A: Physical*, 142(2):561–568, 2008.

[20] James Lenz and S Edelstein. Magnetic sensors and their applications. *IEEE Sensors journal*, 6(3):631–649, 2006.

[21] Felix A Levinzon. Fundamental noise limit of piezoelectric accelerometer. *IEEE Sensors Journal*, 4(1):108–111, 2004.

[22] Arian Rahimi, Jiyu Wu, Xiaoyu Cheng, and Yong-Kyu YK Yoon. Cylindrical radial superlattice conductors for low loss microwave components. *Journal of Applied Physics*, 117(10):103911, 2015.

[23] Arian Rahimi and Yong-Kyu Yoon. Study on cu/ni nano superlattice conductors for reduced rf loss. *IEEE Microwave and Wireless Components Letters*, 26(4):258–260, 2016.

[24] I Sasada. Orthogonal fluxgate mechanism operated with dc biased excitation. *Journal of Applied Physics*, 91(10):7789–7791, 2002.

[25] Ichiro Sasada and Shoumu Harada. Fundamental mode orthogonal fluxgate gradiometer. *IEEE Transactions on Magnetics*, 50(11):1–4, 2014.

[26] Vishal K Shah and Ronald T Wakai. A compact, high performance atomic magnetometer for biomedical applications. *Physics in medicine and biology*, 58(22):8153, 2013.

[27] Dongna Shen, Jung-Hyun Park, Jyoti Ajitsaria, Song-Yul Choe, Howard C Wikle III, and Dong-Joo Kim. The design, fabrication and evaluation of a mems pzt cantilever with an integrated si proof mass for vibration energy harvesting. *Journal of Micromechanics and Microengineering*, 18(5):055017, 2008.

[28] Kushagra Sinha and Massood Tabib-Azar. 27 pt silicon nitride mems magnetometer for brain imaging. *IEEE Sensors Journal*, 16(17):6551–6558, 2016.

[29] S Tadigadapa and K Mateti. Piezoelectric mems sensors: state-of-the-art and perspectives. *Measurement Science and technology*, 20(9):092001, 2009.

[30] Matthew J Thompson and David A Horsley. Parametrically amplified mems magnetometer. In *Solid-State Sensors, Actuators and Microsystems Conference, 2009. TRANSDUCERS 2009. International*, pages 1194–1197. IEEE, 2009.

[31] Tsuyoshi Uchiyama, Norihiko Hamada, and Changmei Cai. Highly sensitive cmos magnetoimpedance sensor using miniature multi-core head based on amorphous wire. *IEEE Transactions on Magnetics*, 50(11):1–4, 2014.

[32] Cornelis A Van Eysden and John E Sader. Resonant frequencies of a rectangular cantilever beam immersed in a fluid. *Journal of applied physics*, 100(11):114916, 2006.

[33] Pei-hong Wang, Kai Tao, Zhuo-qing Yang, and Gui-fu Ding. Resin-bonded ndfeb micromagnets for integration into electromagnetic vibration energy harvesters. *Journal of Zhejiang University SCIENCE C*, 14(4):283–287, 2013.

[34] Xiaosong Wu, Guang Yuan, Seong-O Choi, Yanzhu Zhao, Seong-Hyok Kim, Yong-Kyu Yoon, and Mark G Allen. Lateral lamination approach for multilayer piezoelectric microactuator. *Solid-State Sensor, Actuator, and Microsystems Workshop, Hilton Head Island, SC*, pages 372–375, 2006.

[35] Y-K Yoon, J-H Park, and Mark G Allen. Multidirectional uv lithography for complex 3-d mems structures. *Journal of microelectromechanical systems*, 15(5):1121–1130, 2006.

[36] Yong-Kyu Yoon. Multiferroics for frequency agile microwave applications. *The Journal of Korean-American Scientists and Engineering Association*, 42(1):37–39, 2013.

[37] Yong-Kyu Yoon, J Stevenson Kenney, Andrew T Hunt, and Mark G Allen. Low-loss microelectrodes fabricated using reverse-side exposure for a tunable ferroelectric capacitor application. *Journal of Micromechanics and Microengineering*, 16(2):225, 2005.

[38] Yong-Kyu Yoon, Dongsu Kim, Mark G Allen, J Stevenson Kenney, and Andrew T Hunt. A reduced intermodulation distortion tunable ferroelectric capacitor-architecture and demonstration. *IEEE transactions on microwave theory and techniques*, 51(12):2568–2576, 2003.

[39] Lamia Znaidi. Sol–gel-deposited zno thin films: a review. *Materials Science and Engineering: B*, 174(1):18–30, 2010.

BAA number HR001117S0025

Lead Organization University of Florida

Type of organization Large Organization

Proposers internal reference number

Team members :

PI Jenshan Lin University of Florida

Co-PI Changzhi Li Texas Tech University

Co-PI YK Yoon University of Florida

Co-PI Joaquin Casanova University of Florida

Proposal title Biomimetic microfabricated magnetic gradiometer

Technical PoC :

Casanova, Joaquin

1064 Center Dr, 565 NEB, Gainesville, FL 32611

352-246-9649, jcasa@ufl.edu

Administrative PoC :

Steven Blodgett

1064 Center Dr, 216 LAR, Gainesville, FL 32611

352-846-3948, blodgetts@ece.ufl.edu

Total funds requested

Submitted 06/01/2017

Award instrument requested Cost-Plus-Fixed Fee (CPFF), Cost-contractno fee, cost sharing contractno fee,or other type of procurement contract (specify) or Other Transaction

Place(s) and period(s) of performance: Univeristy of Florida, Texas Tech University, 10/01/2017-4/01/2021

Total proposed cost separated by basic award and option(s), if any, by calendar year and by government fiscal year

Defense Contract Management Agency (DCMA) administration office (if known) Name, address, and telephone number

Defense Contract Audit Agency (DCAA) audit office (if known) Name, address, and telephone number

Date proposal was prepared

DUNS

TIN

CAGE

Subcontractor Information

Proposal validity period (120 days is recommended)

Any Forward Pricing Rate Agreement other such approved rate information, or such documentation that may assist in expediting negotiations (if available). Attachment 1, the Cost Volume Proposer Checklist, must be included with the coversheet of the Cost Proposal.

11 Detailed Cost Breakdown

Task	Phase 1	Phase 2	Phase 3	Total
Sensor Design				
Microfabrication				
Circuit				
Total				

Table 4: Cost breakdown by task

Category	Phase 1	Phase 2	Phase 3	Total
Salaries and fringe				
Travel				
Tuition				
Supplies				
Software				
Fabrication				
Indirect				
Subcontract				
Total				

Table 5: Cost breakdown by category

12 Fundamental Research

Written justification required per Section II.B, Fundamental Research, pertaining to prime and/or subcontracted effort being considered Contracted Fundamental Research.